Journal of Porous Materials (2022) 29:1639–1648
https://doi.org/10.1007/s10934-022-01278-2

Integrated gas expansion and activation strategy to prepare shaddock peel-derived nitrogen doped honeycomb carbon for high performance supercapacitor

Shi-Jia Long[1] · Chang-Dai Si[1]

Accepted: 28 May 2022 / Published online: 21 June 2022

Abstract
Shaddock peel-derived nitrogen doped honeycomb carbon (NHPC) has been prepared by a facile integrated gas expansion, activation and nitrogen doping strategy using urea and potassium carbonate (K_2CO_3) as the mixed activating agents. The thermal decomposition of urea to generate ammonia plays a dual role of a nitrogen source and gas expanding agent, while the K_2CO_3 plays a pore-creating medium. The NHPC exhibits honeycomb-like microstructure feature and possesses a large specific surface area (1438.5 $m^2\ g^{-1}$), high nitrogen doping (6.23 wt%) and well-developed mesopores. Consequently, the NHPC used as electrode for supercapacitor exhibits high specific capacitance of 225 F g^{-1} at 0.25 A g^{-1} and good rate capability. In addition, the symmetric supercapacitor fabricated with NHPC material in 1 M K_2SO_4 aqueous electrolyte delivers high energy density of 18 W h kg^{-1} operated in the wide voltage of 2.0 V and superior cyclability of 97.8% capacity retention after 30,000 cycles.

Keywords Shaddock peel · Integrated activation · Nitrogen doping · Honeycomb carbon · Supercapacitor

1 Introduction

With the growing demand for environmental friendliness and sustainable development, the conversion of renewable biomass into porous carbon materials has attracted great attention in various novel energy conversion and storage applications [1]. Natural biomass has been widely investigated in view of their low cost, easy availability, and unique naturally formed microstructure [2, 3]. For a decade or so, multifarious biomass-derived carbon materials have been widely exploited and used in adsorption, catalyst carrier and electrode materials for batteries/supercapacitors because of the natural abundance and inherent unique architecture of biomass [4–6]. Researchers mainly consider the improvement from the aspects of proper carbon precursors, optimization of activation method and procedure, and heteroatom doping [6, 7]. Studies have shown that the surface wettability and electrical conductivity of carbon materials can be improved by introducing heteroatoms into the carbon skeleton and inducing active sites, thereby increasing the specific capacity of carbon materials [7, 8]. Therefore, to realize the regulation of atomic/electronic structures and properties of biomass-derived carbon materials, it is usually simultaneous pyrolysis of natural biomass and heteroatom-rich precursors to prepare heteroatom-doped carbon materials [9]. In addition, well-developed porous structure is one of the key factors to realize the high performance of carbon materials, which can usually be achieved by rational design experimental procedures and adopt activation methods, including physical steam activation or chemical activator activation (KOH, $ZnCl_2$, etc.) [10–13]. It is well known that conventional physical/chemical activation methods are mainly aimed at increasing the specific surface area and microporosity of carbon materials, but it is difficult to generate predictable porous structures (such as interconnected carbon framework and honeycomb-like carbon) [5]. Thus, the fabrication of biomass-derived heteroatom doped carbon materials with well-developed and interconnected open-pore structures not only requires consideration of biomass materials source and its own microstructural features, as well as

✉ Chang-Dai Si
sicd2008@126.com

[1] College of Chemical Engineering and Technology, Tianshui Normal University, Tianshui 741000, People's Republic of China

character of heteroatom-rich precursors, but also requires rational design of the corresponding synthetic strategies.

Shaddock is widely grown in subtropical and tropical regions, with an annual output of more than 15 million tons worldwide. At the same time, a large amount of plant waste (shaddock peel) produced subsequently has no widespread commercial use [14]. Most of shaddock peels are directly discarded or composted [15], which is undoubtedly a huge waste of biological resources and a negative impact on environment. In particular, the mesocarp of shaddock is mainly a combination of lignin and cellulose, which is a three-dimensional, highly cross-linked polysaccharide polyphenol polymer and polysaccharide [15, 16]. This large network of interconnected cellulose fibrils is great potential precursor for the formation of interconnected carbon framework. In addition, grapefruit peel is a renewable material suitable for mass production. In view of the unique structure properties, there has been some research on grapefruit peel-derived carbon materials for Li–S batteries, supercapacitors and zinc-bromine flow batteries [16–18]. However, those obtained carbon materials suffer from low specific surface area and undeveloped pore structures, which seriously affected the electrochemical properties of carbon materials in energy storage applications, especially in supercapacitors. Therefore, there are still challenges for the preparation of nitrogen doped porous carbon materials with honeycomb-like open-network structure from shaddock peel for electrochemical energy storage applications.

Herein, we carried out a facile integrated gas expansion, activation and nitrogen doping strategy to fabricate shaddock peel-derived nitrogen doped honeycomb carbon (NHPC) from shaddock peel residues, in which the urea and potassium carbonate (K_2CO_3) are employed as the mixed expanding agent and activating agents to regulate pore structure parameters and nitrogen doping effect of carbon materials. The as-prepared NHPC exhibits honeycomb-like microstructure feature and possesses a large specific surface area, high nitrogen doping and well-developed mesopores structure, thereby resulting in excellent electrochemical performance. Furthermore, a symmetric supercapacitor fabricated based on NHPC material as electrodes and 1 M K_2SO_4 aqueous solution as electrolyte exhibits high specific energy operated in the voltage range of 2.0 V, as well as outstanding cyclability during 30,000 cycles.

2 Experimental section

2.1 Materials

Shaddock peel (the shaddock is grown in Fujian province of China), urea and potassium carbonate (K_2CO_3) were purchased from Aladdin Reagent Co., Ltd., China. All the chemical reagents were in analytical grade and used as received directly.

2.2 Preparation of shaddock peel-derived nitrogen doped honeycomb carbon (NHPC)

Shaddock peel was soaked in 0.1 M HCl solution for 24 h and thoroughly washed with distilled water several times, and then dried and following smashed into powder with a mechanical pulverizer. In a typical pyrolysis procedure, the mixture of dry shaddock peel powder (3.0 g), urea (2.0 g) and K_2CO_3 (2.0 g) was put into a tube furnace and heated to 900 °C for 2 h at a heating rate of 3 °C min^{-1} under N_2 atmosphere. After being naturally cooled, the resulting carbide was washed with 2 M HCl to remove inorganic salts, and then washed with ethanol and distilled water thoroughly. The obtained black powder was dried in an air-circulating oven at 60 °C for 12 h and denoted as NHPC.

As comparison, shaddock peel powder was carbonized at 900 °C directly for 2 h under N_2 flow with heating rate of 3 °C min^{-1}, and the resulting carbon material is termed as PPC. Moreover, the mixture of shaddock peel powder (3.0 g) and urea (2.0 g) or mixture of shaddock peel powder (2.0 g) and K_2CO_3 (2.0 g) were pyrolysis as the same procedures of NHPC, the obtained carbon materials were denoted as N-PPC (urea-treated) and P-PPC (K_2CO_3-treated), respectively.

3 Results and discussion

3.1 Mechanism of the formation of the NHPC material

The pericarp-derived nitrogen doped honeycomb carbon (NHPC) was fabricated though facile integrated gas expansion, activation and nitrogen doping strategy by using shaddock peel as carbon precursor and a mixture of urea and potassium carbonate (K_2CO_3) as the mixed activating agents (Fig. 1). The vaporization expansion, activation, carbonization and nitrogen doping of the mixed precursors were completed in one step by high temperature pyrolysis under N_2 atmosphere.

During the graphitization, molten urea and K_2CO_3 are infiltrated into the interior of the shaddock peel, subsequent the thermal decomposition of urea to generate ammonia (NH_3) plays a dual role of a nitrogen source and gas expanding agent in the whole system [19], while the K_2CO_3 plays a pore-creating medium during the high temperature pyrolysis procedure to create an interconnected network structure, resulting in formation of nitrogen doped honeycomb-like carbon framework with well-developed meso- and macropores [20]. With the increase of carbonization temperature,

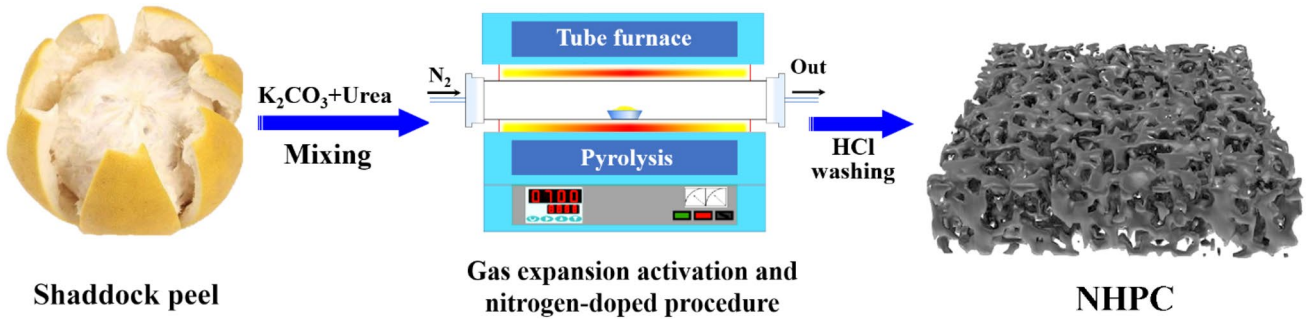

Fig. 1 Schematic illustration for preparation of NHPC material

K_2CO_3 can be decomposed into K_2O and CO_2 (Eq. (1)). In addition, the resulting CO_2 and potassium compounds (K_2CO_3 and K_2O) can be further reduced by carbon (C) to metallic potassium [Eqs. (2)-(4)], which will etch the carbon skeleton [21].

$$K_2CO_3 \rightarrow K_2O + CO_2 \quad (1)$$

$$CO_2 + C \rightarrow 2CO \quad (2)$$

$$K_2CO_3 + 2C \rightarrow 2K + 3CO \quad (3)$$

$$K_2O + C \rightarrow 2K + CO \quad (4)$$

For this physical and chemical activation process, the carbon lattice expands irreversibly, leading to the formation of high microporosity. Therefore, biomass-derived nitrogen-doped porous carbons prepared by a strategy of mixing nitrogen-rich precursors with vapor expansion effect and inorganic salt activators are expected to possess well-developed pores, high specific surface area, connected carbon network morphology, and efficient nitrogen doping miscellaneous.

3.2 Morphology and microstructure characterization

Scanning electron microscopy (SEM) images in Fig. 2 exhibit the morphology and microstructure of the PC, NPC, PPC and NHPC materials. As shown in Fig. 2a, the PC prepared by directly pyrolysis of shaddock peel powder displays large carbon blocks, which were dense and without obvious macropores in the bulk carbon. The NPC prepared by treatment with urea alone have chapped irregularly stacked nanosheets on the surface of the carbon block (Fig. 2b), which is caused by the gas expansion effect of the thermal decomposition of urea to generate NH_3 gas [16, 19]. The PPC prepared by treatment with K_2CO_3 alone possess 3D coralloidal porous carbon skeleton with independent macropores throughout all the bulk materials (Fig. 2c).

Similarly, the NHPC has an interconnected honeycomb-like network structure with thin and wrinkle pore walls, as well as well-developed holes (Fig. 2d). It can be reasonably inferred that both the urea gas expanding and K_2CO_3 pore-creating processes play vital roles in fabricating interconnected framework-like structure. The unique open-macroporous structures are of benefit to the accessibility of electrolytes and transportation of ions in interior of carbon materials [22]. The transmission electron microscope (TEM) image further confirmed this highly interconnected honeycomb-like structure of NHPC material (Fig. 2e), which are consistent with the SEM result. In addition, the high-resolution TEM (HR-TEM) can clearly see the can clearly see the amorphous carbon layer and ultrathin wrinkle edges (Fig. 2f). The results also show that this highly interconnected network structure can stabilize the nanoframe structure.

The porous structure of the PC, NPC, PPC and NHPC materials was measured by nitrogen adsorption–desorption isotherms, and the results are shown in Fig. 3a. All carbon materials show type IV isotherms with hysteresis loops at the relative pressure of 0.5–1.0 P/P_0, signifying that they have a certain amount of mesoporous structures and macroporous structures [23]. The adsorption volume of NHPC is the largest among all carbon materials, indicating that vapor expansion and activation treatments can significantly increase the porosity of carbon materials. Figure 3b shows the pore size distribution of the PC, NPC, PPC and NHPC materials calculated by using the Barrett-Joyner-Halenda (BJH) method, which are mainly centered in the range of 2–7 nm, indicating the existence of superior mesoporous structures [24]. The specific Brunauer–Emmett–Teller (BET) surface area and pore structure parameters of the as-prepared PC, NPC, PPC and NHPC materials are shown in Table 1. The specific surface area (S_{BET}) and specific pore volume of NHPC material are 1438.5 $m^2\ g^{-1}$ and 0.51 $cm^3\ g^{-1}$, respectively, higher than that of the PC (327.1 $m^2\ g^{-1}$, 0.17 $cm^3\ g^{-1}$), NPPC

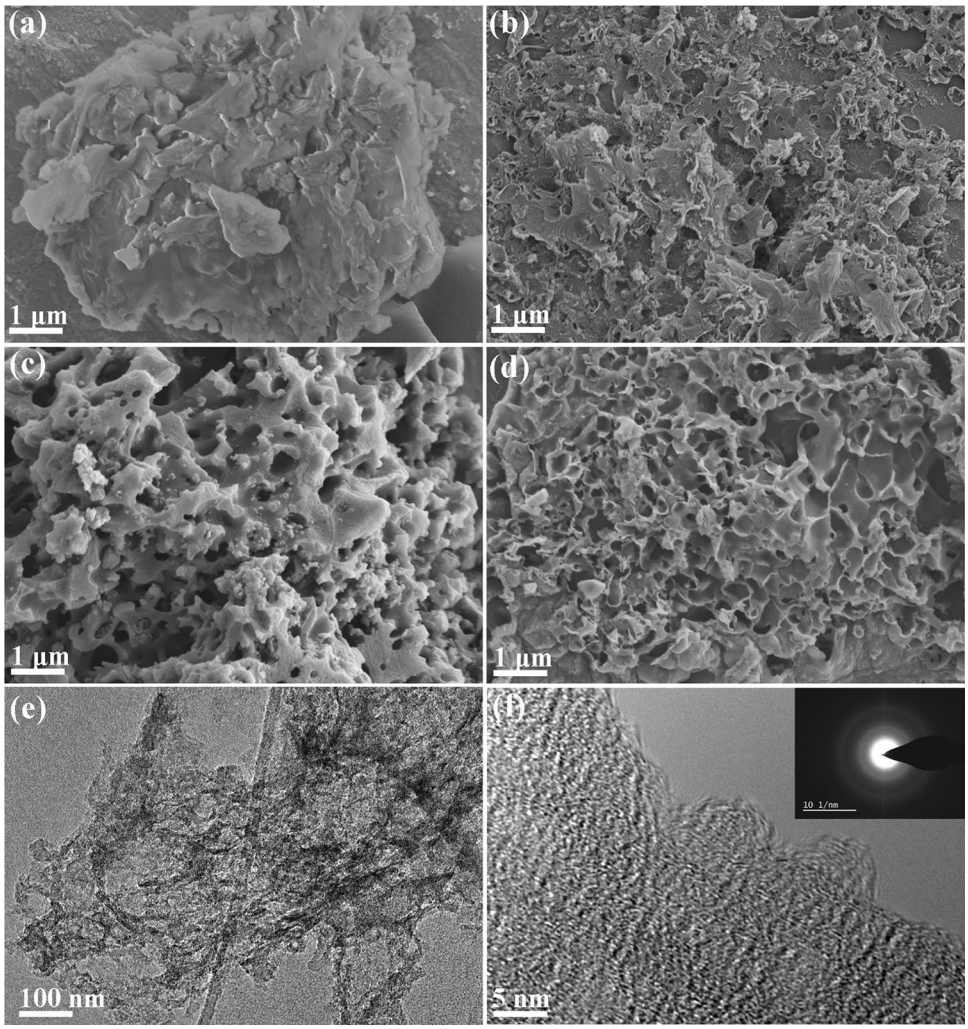

Fig. 2 SEM images of **a** PC, **b** NPC, **c** PPC, **d** NHPC, **e** TEM image and **f** HR-TEM image of NHPC

(559.6 $m^2\ g^{-1}$, 0.25 $cm^3\ g^{-1}$), and PPC (1269.4 $m^2\ g^{-1}$, 0.42 $cm^3\ g^{-1}$) martials. It can be found that the carbon material is treated with urea or K_2CO_3 alone, both NPC and PPC exhibit a relatively lower specific surface area and pore volume than NHPC material treated with mixed activating agents (Table 1). In addition, the specific surface area of PC and NPC obtained by direct carbonization or urea treatment alone, respectively, is largely derived from their micropore surface area (S_{mic}). This result also indirectly indicates that the activation of biomass-based carbon precursors by K_2CO_3 is beneficial to the generation of mesoporous structures. Previous studies have confirmed that the large accessible specific surface area and abundant mesoporous structures are beneficial to the penetration of electrolytes and the adsorption of ions, thereby significantly enhancing the electrical double-layer capacitance [25].

XRD patterns and Raman spectra were carried out to reveal the crystal structure and graphitized microstructure of PC, NPC, PPC and NHPC materials, as shown in Fig. 3c and d, respectively. The XRD patterns of all samples are similar, which exhibit two weak peaks at about 23° and 40°, corresponding to {002} and {100} planes of amorphous graphitic carbon, respectively [26]. From the Raman spectra, the PC, NPC, PPC and NHPC materials have two weak peaks at about 1340 cm^{-1} (D-band) and 1585 cm^{-1} (G-band), which is ascribed to the defect-induced structure induced sp^3-bond carbon atoms and the amorphous sp^2-bonded forms of carbon, respectively [27]. The intensity ratios D-band and G-band (I_D/I_G) for PC, NPC, PPC and NHPC materials are calculated to be 1.04, 1.03, 1.02 and 1.03, respectively, indicating all the carbon materials are composed of a partially disordered carbon and graphitized carbon structure. In addition, the nitrogen doping effect of ammonia gas generated by urea decomposition also increases the microstructural defects of carbon materials.

Figure 3e shows the surface composition of the typical NHPC material, which was studied by XPS. It was confirmed that the O1s, N1s and C1s signals at 531.9, 399.8 and 284.8 eV, respectively, exist in the NHPC material (Fig. 3e). As for the N 1 s spectrum in Fig. 3f, there are show four

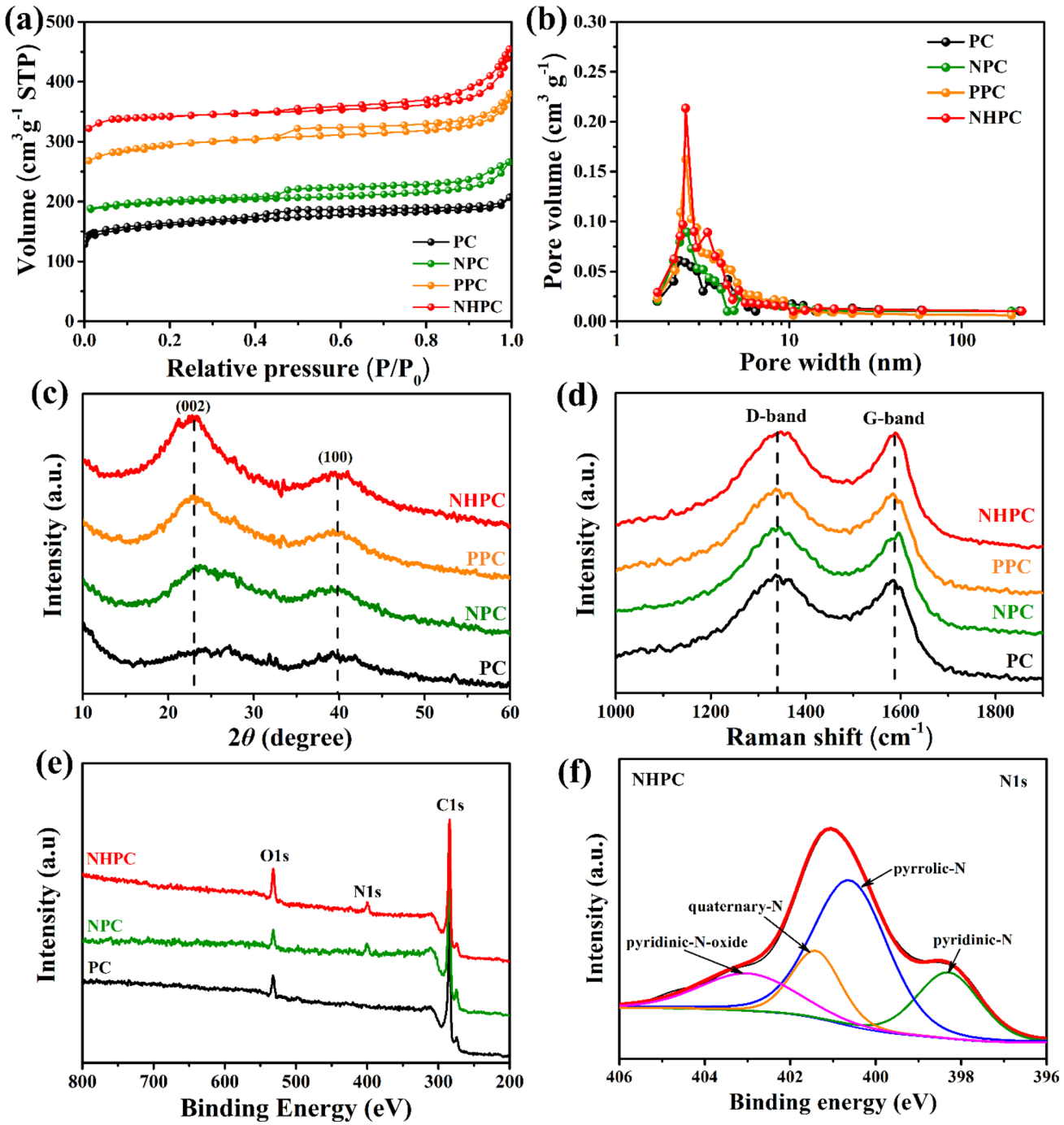

Fig. 3 **a** Nitrogen adsorption–desorption isotherms and **b** pore size distribution curves of the PC, NPC, PPC and NHPC materials. **c** XRD patterns and **d** Raman spectra of the PC, NPC, PPC and NHPC materials. **e** XPS survey spectrum of PC, NPC and NHPC materials. **f** high-resolution N1s

types of nitrogen binding: pyridinic-N (N-6, 398.3 eV), pyrrolic-N (N-5, 400.6 eV), quaternary-N (N-Q, 401.4 eV), and pyridinic-N-oxide (N-X, 403.1 eV) [28], respectively. For the high-resolution XPS spectra of C1s in NHPC material (Figure S1), four peaks at 284.7, 285.4, 286.4 and 288.3 eV are ascribed to C–C (sp^3), C–C (sp^2), C–O and C=O bonds [29], respectively. In addition, elemental analysis (Table 1) reveal that there are over 6.2 wt% N-doped content in both NPC and NHPC, which were prepared by urea treatment. This result further suggests that the combined method of simultaneous gas expansion and activation can provide efficient nitrogen doping for the carbon framework. Therefore, it

Table 1 Elemental analysis and pore structure parameters of the as-prepared carbon materials

Samples	Elemental analysis			S_{BET}[a] ($m^2\ g^{-1}$)	S_{mic}[b] ($m^2\ g^{-1}$)	V_{pore}[c] ($cm^3\ g^{-1}$)	D[d] (nm)
	C %	N %	H %				
PC	69.1	0	1.3	327.1	248.8	0.17	2.4
NPC	70.3	6.52	1.4	559.6	291.5	0.25	2.5
PPC	78.2	0	1.3	1269.4	263.9	0.42	2.8
NHPC	79.9	6.23	1.4	1438.5	254.7	0.51	2.9

[a]Specific surface area determined according to BET method

[b]Micropore surface area from t-plot method

[c]Specific pore volume

[d]Adsorption average pore diameter

can be speculated that NHPC material not only has abundant nitrogen doping effect to enhance the surface wettability and pseudocapacitor behavior [30], but also the interconnected porous structure also shortens the ion diffusion path and enhances the ion buffer storage space, which provides the necessary for the excellent performance of electrode materials for supercapacitor spectrum of NHPC material.

3.3 Electrochemical performance of the carbon materials

The electrochemical performance of the as-prepared carbon materials is evaluated by cyclic voltammetry (CV) and galvanostatic charge/discharge (GCD) techniques at a three-electrode system in 3 M KOH electrolyte. As presented in Fig. 4a, the CV plots of the PC, NPC, PPC and NHPC materials at a scan rate of 50 mV s^{-1} in the operating voltage from − 1.0 to 0 V are show rectangular-like shape, indicating rapid electrons/ions transfer and typical double layer capacitive characteristics. However, the CV plots of both NPC and NHPC materials show a hump shape during − 0.7 to − 0.2 V, which deviates from the rectangular shape, meaning the materials have certain redox pseudocapacitive behavior characteristics. One can see that the order of their electrochemical areas is: NHPC > PPC > NPC > PC, which indicates that the NHPC material has a largest specific capacitance, because the electrochemical active area is proportional to the specific capacitance. In addition, we can also find that the electrochemically active area of PPC is significantly larger than that of NPC, indicating that the improvement of pore structure contributes more significantly to the specific capacitance of carbon materials, although nitrogen doping can provide pseudocapacitive effects in carbon materials. In Fig. 4b, the CV plots of NHPC material at various scan rate from 10 to100 mV s^{-1} retain a stable rectangular-like shapes, verifying it possesses excellent rate capability.

The GCD plots of the various carbon materials examined at current density of 0.25 A g^{-1} shown that the NHPC material has longest charge/discharge times among those materials (Figure S2), demonstrating it has a largest specific capacitance, in consistent with CV results. The GCD test of NHPC material were carried out at various current densities ranging from 0.5 to 20 A g^{-1}, as shown in Fig. 4c. All GCD plots has highly symmetrical at various current densities, meaning that NHPC material possesses excellent electrochemical reversibility. The specific capacitances of the PC, NPC, PPC and NHPC materials are calculated from galvanostatic discharge plots (Supporting information) and the corresponding capacitances at various current densities are presented in Fig. 4d. For the NHPC material, the specific capacitance is reach to 225 F g^{-1}, which value is larger than that of PC (128 F g^{-1}), NPC (169 F g^{-1}) and PPC (188 F g^{-1}) under the same current density of 0.25 A g^{-1}. Moreover, the specific capacitance of NHPC is 216, 207, 193, 185 and 173 F g^{-1}, at various current densities of 0.5 1, 3, 5 and 10 A g^{-1}, respectively. It even remains high capacitance retention of 71% (160 F g^{-1}) at a high current density of 20 A g^{-1}, superior to other as-prepared carbon materials yet (Fig. 4d). The excellent electrochemical performance of NHPC electrode material is attributed to the combination of the large specific surface area, highly interconnected porous structure and abundant mesoporous in carbon framework, as well as the high nitrogen doping content. Electrochemical impedance spectroscopy (EIS) measured were performed to further evaluate the electrochemical properties of carbon materials (Figure S3). The NHPC electrode possesses a small internal series resistance (Rs) and charge transfer resistance (R_{ct}) compared to other carbon materials, because it has a small real axis (Z′) intercept and semicircle in the high frequency region. According to the Nyquist plots of carbon materials, the electrical conductivity of PC, NPC, PPC and NHPC is 0.72 S m^{-1}, 0.85 S m^{-1}, 1.14 S m^{-1} and 1.21 S m^{-1}, respectively.

For practical applications, a symmetric supercapacitor (SC) device was assembled with NHPC as electrode material to further measure its electrochemical performance. According to the energy density formula of supercapacitor $E = 1/2CV^2$, it can be known that improving the energy density (E) of the device can be achieved by increasing the operating voltage (V) of the device under the condition of

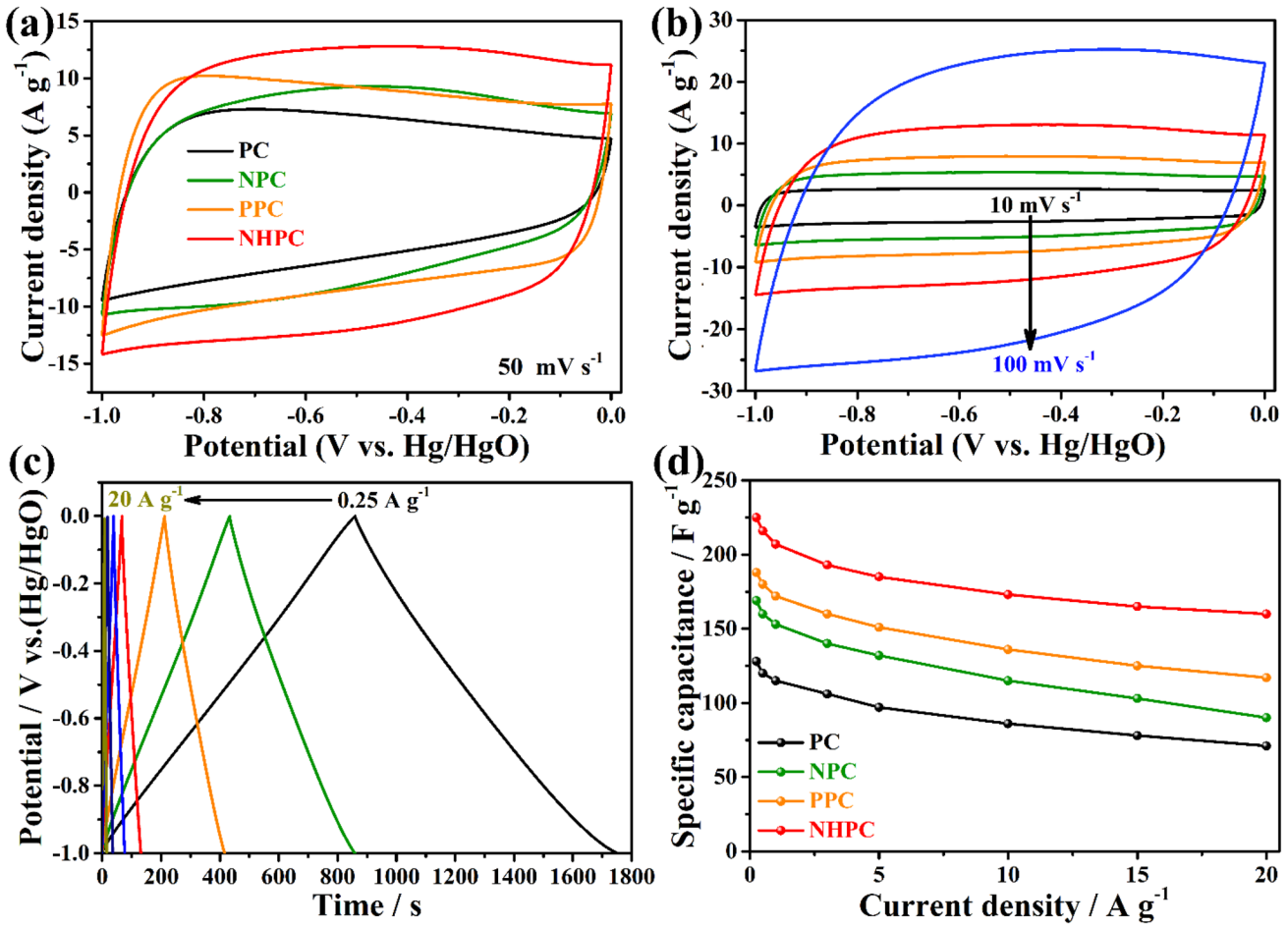

Fig. 4 **a** CV plots of the PC, NPC, PPC and NHPC materials, **b** CV plots of NHPC electrode material at various scan rates, **c** GCD plots of the NHPC material at various current densities, **d** specific capacitance of the carbon materials at different current densities

determining the electrode materials. It was reported that carbon-based capacitors based on neutral aqueous electrolyte (such as Na_2SO_4 and Li_2SO_4) exhibits a higher operating voltage than that in acid/alkali electrolytes [31, 32], because neutral electrolytes have low concentrations of H^+ and OH^-, which are difficult to occur hydrogen and oxygen evolution [16]. Thus, the SC based on NHPC electrode material was fabricated in 1 M K_2SO_4 electrolyte in this work. Firstly, the electrochemical stability and operate voltage range of SC device was confirmed and measured at different operating voltage from 1.0 to 2.0 V, as illustrated in Fig. 5a. Indeed, the CV plots of the device can be stabilized over an operating voltage range greater than 1.0 V and retains a perfect rectangular-like shape even when the voltage is extended to 2.0 V, indicating excellent reversibility and stability. Hence, we chose the operating voltage of 2.0 V for the subsequent electrochemical performance tests of SC device with NHPC electrode material. In Fig. 5b, the CV plots of SC device at various scan rate from 10 to 200 mV s^{-1} at operating voltage of 2.0 V maintain a stable rectangular-like shapes, verifying it possesses excellent the electrochemical stability and rate capability. In addition, GCD plots of SC device at various current densities in Fig. 5c indicate that the discharging plots are highly symmetrical with their charging counterpart, demonstrating a high electrochemical reversibility. The Ragone plot of the SC device was calculated from their GCD plots are shown in Fig. 5d. Concretely, the energy density of SC device NHPC electrode materials in 1 M K_2SO_4 electrolyte is as high as 18 Wh kg^{-1} at a power density of 110 W kg^{-1} and still remains at an energy density of 9.3 Wh kg^{-1} at power density of 5000 W kg^{-1} according to the total active material mass. This performance is superior to most of the reported aqueous carbon-based symmetric supercapacitor (Table S1).

Electrochemical impedance spectroscopy (EIS) analysis is an effective technique to deeply study the capacitive behavior of SC device. Nyquist plot of SC device shows a small semicircle in the high frequency region and a vertical line in the low frequency region (Fig. 5e). It can be seen from the inset of Fig. 5e that equivalent series resistance

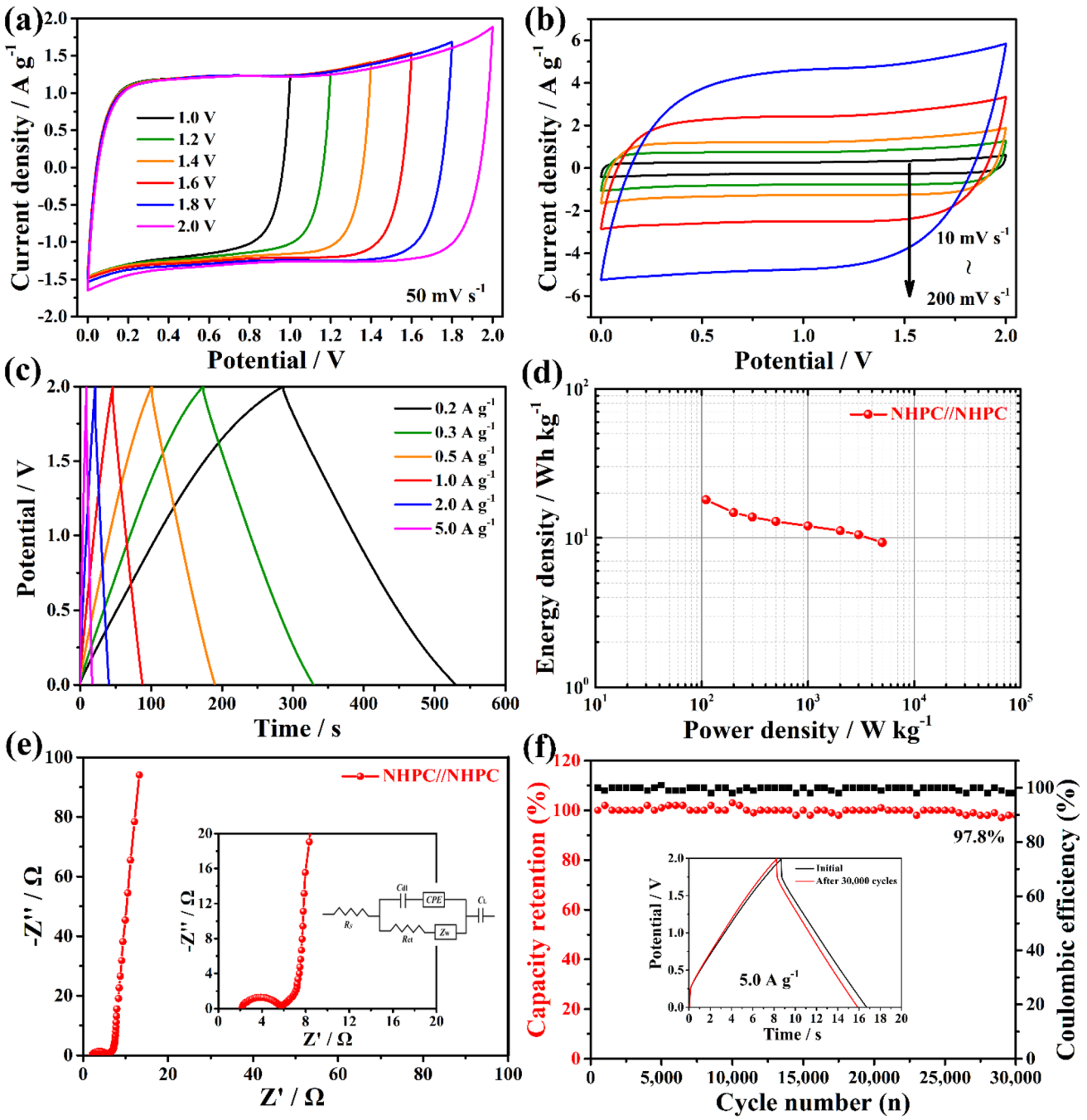

Fig. 5 **a** CV curves of SC device with various potential ranges at 50 mV s^{-1}, **b** CV curves of the SC device at various scan rates; **c** GCD curves of the SC device at various current densities, **d** Ragone plot of the SC device, **e** Nyquist plot of SC device (inset of the equivalent circuit). **f** cyclic stability and columbic efficiency of the SC device at 5 A g^{-1}

of SC device is 1.9 Ω calculated from the intercept of the semicircle with the Z′ axis in a high frequency, while the charge transfer resistance is 4.1 Ω calculated from diameter of the semicircle [33]. The corresponding equivalent circuit from Nyquist plot is as shown in the inset of Fig. 5e, where R_s stands for an internal resistance of the electrolyte and electrode, R_{ct} is the charge transfer resistance. The transition from the semicircle to the long tail of vertical curve is called the Warburg resistance (Z_W) and is a result of the frequency dependence of ion diffusion/transport in the electrolyte to the electrode surface, *CPE* is the constant phase element, C_{dl} is the double-layer capacitance, C_L is the limit capacitance [34]. The nearly vertical line (large slope) in the low frequency describes a low diffusive resistance of electrolyte

in the SC device. The cycling stability of the SC device was investigated for 30,000 cycles at 5 A g^{-1} in Fig. 5f. The specific capacitance of the SC device decreases slightly with the increase of the number of charge/discharge cycles, and maintained a wonderful capacity retention of 97.8% of the initial value after 30,000 cycles. It can see that the coulombic efficiency of the SC device is also stable at 100%. In addition, the resistance value of the device increases slightly after 30,000 cycles (Figure S4). It is shown that the N-PMNC electrode material has outstanding electrochemical reversibility and stability even at a high operating voltage of 2.0 V in aqueous electrolyte. The SC device achieves a remarkable performance can be attributed to the honeycomb-like microstructure feature, large specific surface area, well-developed mesopores structure and high nitrogen doping in NHPC electrode material. All of these results verify excellent electrochemical performance and great potential applications for the aqueous SC device.

4 Conclusions

In conclusion, we successfully prepared a nitrogen doped honeycomb-like carbon (NHPC) using shaddock peel as carbon precursor through an integrated gas expansion, activation and nitrogen doping strategy. The as-prepared NHPC displays interconnected honeycomb-like network structure and possesses a large specific surface area of 1438.5 m^2 g^{-1} and well-developed mesopores structure, as well as high nitrogen doping of 6.23 wt%. These microstructure features not only shorten the ion diffusion path and enhances the ion buffer storage space, but also enhance the surface wettability and pseudocapacitor behavior. Thus, the NHPC electrode material exhibits high specific capacitance of 225 F g^{-1} at 0.25 A g^{-1} and good rate capability. Further, a symmetric supercapacitor fabricated with NHPC electrode materials in 1 M K_2SO_4 aqueous electrolyte carries a wide operating voltage of 2.0 V and delivers high energy density of 18 W h kg^{-1} at high power density of 110 W kg^{-1}, and wonderful capacity retention of 97.8% of the initial value after 30,000 cycles. These results indicate that biomass-derived carbon materials have great application potential in low-cost energy storage devices, and are also expected to be used as hydrogen storage, fuel cell catalyst supports, etc.

Supplementary Information The online version contains supplementary material available at https://doi.org/10.1007/s10934-022-01278-2.

Acknowledgements This work was supported by grants from the Natural Science Foundation of China (No. 21761030), the Science and Technology Plan Projects of Gansu Province (No. 21JR11RE032, 21JR11RE029), the Science and Technology Plan Projects of Tianshui City (No. 2021-FZJHK-6203), the Innovation Fund Project of Tianshui Normal University (No. CXJ2020-23), Gansu Longyuan Youth Innovation and Entrepreneurship Team Project (No.2022-77) and Tianshui Normal University 'QinglanTalents' Project.

Author contributions SL designed the experimental program and complete the experiment. SL and CS wrote the main manuscript text and SL prepared Figs. 1, 2, 3, 4, 5. Changdai Si is providing financial support for the experiment. All authors reviewed the manuscript.

Declarations

Conflict of interest The authors declare that they have no known competing financial interests or personal relationships that could have appeared to influence the work reported in this paper. The authors declare no competing interests.

References

1. J. Wang, X. Zhang, Z. Li, Y. Ma, L. Ma, J. Power Sources **451**, 227794 (2020)
2. W. Tang, Y. Zhang, Y. Zhong, T. Shen, X. Wang, X. Xia, J. Tu, Mater. Res. Bull. **88**, 234–241 (2017)
3. Z. Wang, M.S. Ganewatta, C. Tang, Prog. Polym. Sci. **101**, 101197 (2020)
4. A.T. Hoang, S. Nižetić, C.K. Cheng, R. Luque, S. Thomas, T.L. Banh, V.V. Pham, X.P. Nguyen, Chemosphere **287**, 131959 (2022)
5. J. Deng, M. Li, Y. Wang, Green Chem. **18**, 4824–4854 (2016)
6. Y. Wang, L. Zhao, H. Peng, X. Dai, X. Liu, G. Ma, Z. Lei, Ionics **25**, 4315–4323 (2019)
7. J.P. Paraknowitsch, A. Thomas, Energy Environ. Sci. **6**, 2839–2855 (2013)
8. T. Asefa, X. Huang, Chem. Eur. J. **23**, 10703–10713 (2017)
9. J. Gao, D. Fan, X. Liu, New J. Chem. **45**, 15469–15474 (2021)
10. P.T. Williams, A.R. Reed, Biomass Bioenerg. **30**, 144–152 (2006)
11. J. Pallarés, A. González-Cencerrado, I. Arauzo, Biomass Bioenerg. **115**, 64–73 (2018)
12. J. Wang, S. Kaskel, J. Mater. Chem. **22**, 23710–23725 (2012)
13. M.J. Prauchner, K. Sapag, F. Rodríguez-Reinoso, Carbon **110**, 138–147 (2016)
14. J. Liang, J. Wu, P. Li, X. Wang, B. Yang, Water Treat. **39**, 1–3 (2012)
15. Y. Zhao, X. Yang, B. Wu, J. Shang, Y. Liu, Z. Dai, X. Luo, J. Agric. Food Chem. **67**, 8810–8818 (2019)
16. H. Peng, G. Ma, Z. Sun, Z. Zhang, Q. Yang, Z. Lei, Electrochim. Acta **190**, 862–871 (2016)
17. J. Zhang, J. Xiang, Z. Dong, Y. Liu, Y. Wu, C. Xu, G. Du, Electrochim. Acta **116**, 146–151 (2014)
18. M. Wu, R. Zhang, K. Liu, J. Sun, K. Chan, T. Zhao, J. Power Sources **442**, 227255 (2019)
19. R. Lan, J.T.S. Irvine, S. Tao, Int. J. Hydrog. Energy **37**, 1482–1494 (2012)
20. Y. Xi, Y. Wang, D. Yang, W. Liu, Q. Li, X. Qiu, J. Alloys Compd. **785**, 706–714 (2019)
21. C. Lu, S. Xu, C. Liu, J. Anal. Appl. Pyrol. **87**, 282–287 (2010)
22. J. Ye, P. Simon, Y. Zhu, Natl. Sci. Rev. **7**, 191–201 (2020)
23. C. Buttersack, Phys. Chem. Chem. Phys. **21**, 5614–5626 (2019)
24. L. Shi, L. Liang, F. Wang, M. Liu, K. Chen, K. Sun, N. Zhang, J. Sun, ACS Sustain. Chem. Eng. **3**, 3412–3419 (2015)
25. H. Ji, X. Zhao, Z. Qiao, J. Jung, Y. Zhu, Y. Lu, L. Zhang, A.H. MacDonald, R.S. Ruoff, Nat. Commun. **5**, 3317 (2014)
26. J. Elisadiki, Y.A.C. Jande, T.E. Kibona, R.L. Machunda, Ionics **26**, 2477–2492 (2020)

27. H. Peng, S. Qi, Q. Miao, R. Zhao, Y. Xu, G. Ma, Z. Lei, J. Power Sources **482**, 228993 (2021)
28. Z. Tian, S. Dai, D. Jiang, Chem. Mater. **27**, 5775–5781 (2015)
29. G. Qu, S. Jia, H. Wang, F. Cao, L. Li, C. Qing, D. Sun, B. Wang, Y. Tang, J. Wang, A.C.S. Appl, Mater. Interfaces **8**, 20822–20830 (2016)
30. L. Zhang, X. Zhao, Chem. Soc. Rev. **38**, 2520–2531 (2009)
31. M.P. Bichat, E. Raymundo-Piñero, F. Béguin, Carbon **48**, 4351–4361 (2010)
32. Q. Qu, L. Liu, Y. Wu, R. Holze, Electrochim. Acta **96**, 8–12 (2013)
33. R. Zhao, H. Peng, H. Wang, J. Liang, Y. Lv, G. Ma, Z. Lei, J. Energy Storage **28**, 101174 (2020)
34. J. Chang, M. Jin, F. Yao, T.H. Kim, V.T. Le, H. Yue, F. Gunes, B. Li, A. Ghosh, S. Xie, Y.H. Lee, Adv. Funct. Mater. **23**, 5074–5083 (2013)